In situ monitoring distribution and migration of ^{3}He in liquid-solid ^{4}He mixtures

Zhi Gang Cheng [1,3,4,*] and John Beamish[2,†]

[1]*Beijing National Laboratory for Condensed Matter Physics, Institute of Physics, Chinese Academy of Sciences, Beijing 100190, China*

[2]*Department of Physics, University of Alberta, Edmonton, Alberta T6G 2E1, Canada*

[3]*University of Chinese Academy of Sciences, Beijing 100049, China*

[4]*Songshan Lake Materials Laboratory, Dongguan, Guangdong 523808, China*

Helium is ideal for studies of quantum liquids and solids, with its significant advantage of being extremely pure at low temperatures—all except isotopic impurities are frozen out. However, even tiny concentrations of isotopic impurities have significant effects on both dynamic and thermodynamic properties. Difficulties in predicting and measuring impurities' distributions and motions make it hard to systematically study such effects. Here we report a sensitive technique combining dielectric and pressure measurements to resolve concentration changes of isotopic impurities in liquid helium with a resolution of 40 ppm. Using this technique, we observed that ^{3}He impurities concentrate in liquid phase of solid-liquid coexisting ^{4}He at low temperatures, and their migration between the liquid and solid phases when temperature is changed. This migration process is much slower than ^{3}He diffusion in the liquid phase, suggesting the bottleneck is in the solid phase and possibly transmission across the liquid-solid interface.

The purity of helium makes it an ideal system to experimentally study quantum phenomena in fluids and solids. Almost all impurities are frozen out at ultralow temperatures, the only exception being isotopic impurities. These typically occur at small concentrations, e.g., commercial ^{4}He contains about 300 parts per billion (ppb) of ^{3}He. However, even small concentrations of ^{3}He or ^{4}He impurities can have large effects in helium because of their different quantum statistics. In liquid ^{4}He, even parts per million (ppm) of ^{3}He drastically increase the specific heat of liquid ^{4}He below 1 K, reflecting their added quasiparticle excitation spectrum [1]. Impurity effects can also be important in helium crystals. The shear modulus of solid ^{4}He has a large anomalous increase at temperatures below ≈ 100 mK, which has been ascribed to ^{3}He impurities binding to and immobilizing dislocations, thus effectively stiffening the solid [2,3]. Such an anomaly is discernible even when the ^{3}He concentration is below 1 ppb [4]. Similar effects have also been observed for dilute ^{4}He impurities in solid ^{3}He [5].

Isotopic impurities are extremely large mobile in solid helium because of their large atomic zero-point motion. Thanks to this high mobility, the distribution of impurities is sensitive to local environments and can be highly variable. Recently, considerable attention has been focused on mass flow in solid

helium. The flow, which appears below 0.6 K, is suddenly suppressed at a lower temperature T_d [6–8]. The suppression appears at higher temperature and becomes more obvious when the ^{3}He concentration x_3 is increased from 10^{-7} to 10^{-3}, while it disappears for very small concentration $x_3 < 5 \times 10^{-12}$ [8]. The suppression of flow can exhibit hysteresis on temperature cycling, depending on the experimental setup and x_3. Experiments involving "superfluid leads" (liquid helium confined in a porous glass, Vycor) [6,7,9] exhibit stronger suppression and, for the same x_3, higher T_d than measurements with no liquid helium present [8]. A recent experiment with a micrometer-size solid sandwiched between centimeter-size "superfluid leads" showed no suppression of flow up to $x_3 = 1.5\%$ [10], in contrast with the other experiments involving minimeter- or centimeter-scale solid samples [6–9].

The hysteresis in the flow experiments suggests that ^{3}He impurities are distributed differently, depending on the experimental arrangements and sample histories. Inhomogeneities in the ^{3}He distribution are expected in experiments with liquid and solid helium because of different impurity energies in different environments. Taking solid hexagonal close packing (hcp) ^{4}He lattice as a reference, the energy of a ^{3}He atom bound to a dislocation is $E_{dis}/k_B \approx -0.7$ K [11]. Its energy is lower in liquid ^{4}He, $E_l/k_B = -1.36$ K [12,13], and ^{3}He is even more strongly bound on liquid-solid interfaces $E_{sl}/k_B = -2 \sim -10$ K [14–17]. As the temperature is lowered, impurities tend to concentrate in locations with the deepest potential. Their movement and binding are driven by thermal activations and involve complicated processes of ^{3}He/^{4}He exchange in various phases, making it difficult to precisely predict the dynamics. Experimental measurements of impurity distributions and migration in solid-liquid helium mixtures would

*zgcheng@iphy.ac.cn

†jbeamish@ualberta.ca

be valuable, but are challenging given the small impurity concentrations and lack of direct methods to map their distributions.

Here we describe a technique for *in situ* monitoring of ^{3}He concentrations in liquid ^{4}He. The method is based on precise capacitive measurements of the dielectric constant of liquid helium and supplemented by liquid pressure measurement. The Straty-Adams capacitive pressure gauge has been widely used in previous studies on melting curves of ^{4}He/^{3}He mixtures [18–22], and direct capacitive measurement of dielectric constant has also been applied in certain studies as a scale of liquid density [23,24]. However, these studies involved relatively high ^{3}He concentrations (on the order of a few percent) near or at the saturated ^{3}He concentration in liquid ^{4}He. By using a commercial high-resolution capacitance bridge, our technique has a sensitivity of 40 ppm in measuring ^{3}He concentration, which enables us to study mixtures with much lower concentrations. We applied this technique to study the distribution of ^{3}He impurities in ^{4}He liquid-solid coexisting samples with an average concentration between 1000 and 3000 ppm, and successfully monitored the migration of ^{3}He between solid and liquid. Our observations reveal that the transfer of ^{3}He impurities between liquid and solid ^{4}He is a slow and temperature-dependent process. Analyses suggest ^{3}He diffusion is likely bottle-necked in solid phase and at the liquid-solid interface.

I. DISCRIPTION OF THE TECHNIQUE

The dielectric constant ϵ of a nonpolar material like helium is related to its number density n by the Clausius-Mossotti relation

$$\frac{\epsilon - 1}{\epsilon + 2} = \frac{\alpha n}{3\epsilon_0}, \tag{1}$$

where ϵ_0 is the permittivity of vacuum and α the atomic polarizability. ^{3}He atoms have essentially the same polarizability as ^{4}He atoms [25] but their larger zero-point motion gives liquid ^{3}He a lower number density. Increasing x_3 of a liquid helium mixture lowers its average number density and the resulting drop in its dielectric constant can be detected in capacitance measurements.

Precise capacitance measurements have been carried out in liquid helium using homemade bridges [25–27] or tunnel diode oscillator circuits [28]. These techniques can measure fractional changes of the dielectric constant or capacitance C with a resolution $\frac{\delta\epsilon}{\epsilon} = \frac{\delta C}{C}$ that can reach 10^{-8}, although the measurements were challenging. To demonstrate the practicality and convenience of the method, we sacrificed some resolution and used a commercial ac capacitance bridge (Andeen Hagerling 2500) with a resolution of 5×10^{-7}. Higher resolution measurements are possible using capacitance bridges with long averaging times to reduce noise, but more complicated methods are needed to eliminate drift in reference capacitors and leads.

The resolution of the capacitance bridge determines the sensitivity of the dielectric constant and ^{3}He concentration measurements. Helium atoms' low polarizibility means their contribution to the liquid helium's dielectric constant is small, e.g., at their vapor pressures, $\epsilon_4 \approx 1.06$ and $\epsilon_3 \approx 1.04$ for ^{4}He

and ^{3}He, respectively [26,27]. Since $\frac{\epsilon-1}{\epsilon+2} \ll 1$, the Clausius-Mossotti relation can be approximated by $\epsilon - 1 \approx \frac{\alpha n}{\epsilon_0}$ and the resolution of the dielectric measurement is related to that of the number density by $\frac{\delta n}{n} \approx \frac{\delta\epsilon}{\epsilon - 1}$. For our capacitance bridge with $\frac{\delta C}{C} \approx 5\times10^{-7}$, this gives number density resolution $\frac{\delta n}{n} \approx 10^{-5}$, i.e., 10 ppm.

In the absence of ^{3}He impurities, the density of liquid ^{4}He depends on pressure (via its compressibility κ) and on temperature (via its thermal expansion coefficient α_v). For isothermal pressure changes, the resulting density change is given by

$$\frac{\delta n}{n} = e^{\int_{P_i}^{P_f} \kappa(P)dP} - 1 \approx \int_{P_i}^{P_f} \kappa(P)dP, \tag{2}$$

where P_i and P_f are initial and final pressures and the second approximation is valid for small density changes $|\frac{\delta n}{n}| \ll 1$. The compressibility of liquid ^{4}He has a weak temperature dependence at low temperatures and for pressures close to the melting curve it can be approximated by a constant $\kappa = 4.5\times10^{-3}$ bar^{-1} [29]. For small pressure changes, Eq. (2) can be simplified as $\frac{\delta n}{n} = \kappa \delta P$, and with our capacitance resolution, helium density changes corresponding to pressure changes as small as $\delta P = 2$ mbar can be detected. This cannot compete with the pressure resolution of Straty-Adams capacitive gauges, which can easily resolve pressure changes of 10 μbar, and even 0.5 μbar with an optimized setup [29]. However, such dielectric measurements provide a convenient and sensitive way to measure liquid helium's density and so, by making measurements at different pressures, its isothermal compressibility κ can be determined.

Temperature variations also lead to density changes due to thermal expansion. For isobaric warming from T_1 to T_2, the density change is given by

$$\frac{\delta n}{n} = 1 - e^{\int_{T_1}^{T_2} \alpha_v(T)dT} \approx -\int_{T_1}^{T_2} \alpha_v(T)dT, \tag{3}$$

where α_v is volumetric thermal expansion coefficient and the second approximation is again valid for $|\frac{\delta n}{n}| \ll 1$. The thermal expansion of liquid ^{4}He is dominated by phonons below 0.4 K, where $\alpha_v(T) = 9.0\times10^{-5}T^3$ K^{-4} [29]. The total change in density between 0 and 0.4 K is $\frac{\delta n}{n} = -5.76\times10^{-7}$, well below the resolution of capacitive measurements, but increases rapidly at higher temperatures. By holding the pressure constant and measuring the dielectric constant as temperature is varied, the thermal expansion coefficient α_v can be determined.

Helium's atomic polarizability is essentially independent of temperature below 1 K and is only slightly pressure dependent [25]. For example, when liquid ^{4}He is compressed at low temperature from its saturated vapor pressure up to the melting curve at 25 bar, the polarizability α_4 changes by about 0.03% [25], which is negligible compared to the accompanying 19% change in the density n. To high accuracy, the pressure dependence of α_4 can be ignored, and dielectric measurements are directly related to liquid ^{4}He's number density n.

The atomic polarizabilities of the ^{3}He and ^{4}He isotopes, α_3 and α_4, are almost equal, e.g., $\frac{\alpha_3}{\alpha_4} = 1.000135$ at their
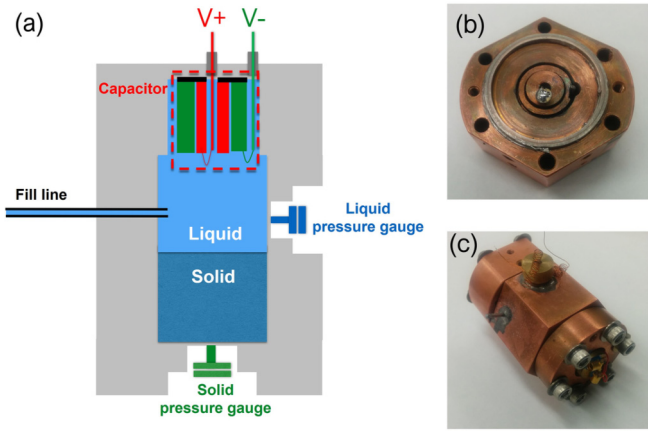
FIG. 1. (a) Schematic drawing of the experimental setup. (b) Picture of the cell's top, with the concentric cylindrical capacitor in the center. (c) Picture of the assembled cell. Two capacitive pressure gauges and the inlet capillary can be seen.

FIG. 2. (a) Melting pressure of the pure ^{4}He sample with a solid fraction of 34% between 16 and 850 mK. The red dashed line is a fitting curve in the form of $P(T) = P(0) - AT^4$ with $P(0) = 25.4$ bar with $A = 0.032424$ bar/K^4. (b) Temperature dependence of the capacitance of the concentric liquid density capacitor. The value for an empty cell was $C_e = 8.66543$ pF at 16 mK, and it increased to $C = 9.25709$ pF after the sample was made. The increase due to filling of liquid helium in the gap was $\Delta C = C - C_e = 0.59166$ pF. The red dashed line represents the fitting using Eq. (4), and the orange and olive dashed lines represent the calculated capacitance change contributed by pressure change and thermal expansion, respectively.

saturated vapor pressures [25]. For most measurements, the small difference between α_3 and α_4 can be ignored. In isotopic mixtures, the dielectric constant is then determined simply by the average number density n. When ^{3}He impurities are added to pure ^{4}He, their effect on the liquid's dielectric constant is just due to the difference between the isotopes' atomic volumes. At low temperature and saturated vapor pressure, pure ^{3}He has a molar volume of 36.5 cm^3/mol, compared to liquid ^{4}He at 27.6 cm^3/mol and the corresponding dielectric constants are related by $(\frac{\epsilon-1}{\epsilon+2})_{3\text{He}} = 1.401 \times 10^{-2}$ and $(\frac{\epsilon-1}{\epsilon+2})_{4\text{He}} = 1.851 \times 10^{-2}$ [26]. If we assume that a ^{3}He impurity occupies the same volume in liquid ^{4}He as an atom in liquid ^{3}He, then a capacitive measurement with a density resolution $\frac{\delta n}{n} \approx 10$ ppm corresponds to an impurity concentration resolution of about 40 ppm.

II. TEST ON PURE ^{4}He WITH LIQUID AND SOLID IN COEXISTENCE

In order to demonstrate the technique in practice, we first used it in liquid ^{4}He in coexistence with solid phase in the temperature range from 16 to 850 mK. The experimental cell is shown in Fig. 1. A concentric cylindrical capacitor is integrated into the top of the cell [shown in Fig. 1(b)]. Two capacitive pressure gauges are located in the upper half on side wall and at the bottom center to monitor pressures in the liquid and solid phases respectively. Liquid helium is admitted into the cell via a capillary entering the side wall, initially kept at a higher temperature, pressurized, and cooled down to partially freeze. By adjusting the initial liquid pressure before samples start to freeze, the solid ^{4}He fraction is controlled to be less than 60%, to avoid having solid covering the liquid pressure gauge. Since liquid and solid coexist in the cell, the liquid is always at the melting curve pressure, so there is no need for other pressure control. The melting curve of ^{4}He exhibits a shallow pressure minimum (about 8 mbar deep) at about 0.78 K, in contrast to that of ^{3}He, which has a much deeper minimum (about 4 bar) around 0.32 K. At low temperatures, where phonons are the only thermal excitations in the liquid
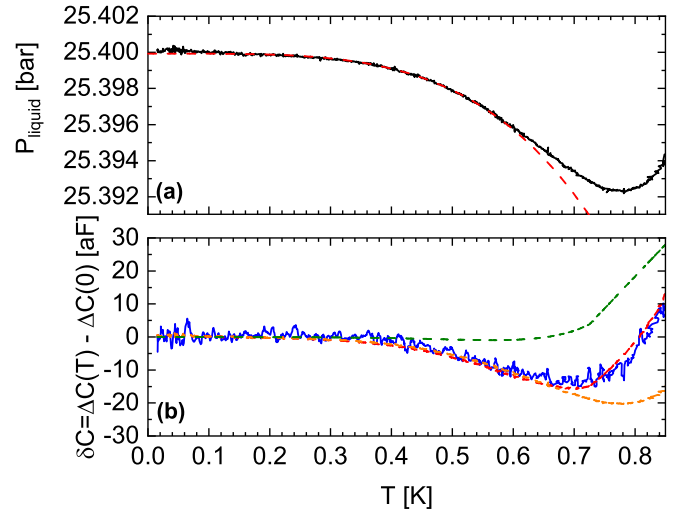
and solid, ^{4}He's melting curve pressure depends on temperature as $P(T) = P(0) - AT^4$.

The ^{3}He concentration in the commercial ^{4}He gas used to fill the cell is 120 ppb, so the impurities' effect on the dielectric constant is far below our resolution and the sample can be considered as pure ^{4}He. Any observable capacitance change ($\Delta C = C - C_{\text{empty}} \propto \epsilon - 1 \propto n$, considering $\frac{\epsilon-1}{\epsilon+2} \approx \frac{\epsilon-1}{3}$) is due to density variations from pressure changes along the melting curve and thermal expansion. The change can be written as

$$\Delta C(T) = \Delta C(0)\left[1 + \kappa(P(T) - P(0)) - \int_0^T \alpha_v(T)\,dT\right].$$

(4)

Simultaneous measurements of the pressure and the liquid dielectric constant were carried out using the capacitive pressure gauge (with a resolution of about 0.1 mbar) and the cylindrical density capacitor. Results are shown in Fig. 2. The temperature dependence of the melting pressure agrees with theoretical expectations and with previous measurements, showing a T^4 decrease (the red dashed line) at temperatures up to about 0.6 K, and a minimum at around 0.78 K. The T^4 decrease at low temperatures is attributed to the phonon entropy in the solid (contributed by one longitudinal and two transverse modes), which is larger than that in the superfluid (with only one longitudinal mode); phonon densities in both phases have a T^3 dependence. The slope becomes positive above 0.78 K where the liquid's entropy surpasses the solid's as roton excitations start to play a role.

The blue curve in Fig. 2(b) is the measured values from the cylindrical liquid density capacitor. Contributions to this capacitance from both pressure variation and thermal expansion are calculated based on Eq. (4) and are separately shown by orange and green dashed lines respectively. The calculations use the measured pressure in Fig. 2(a) and volume thermal expansion coefficient $\alpha_v(T)$ from Ref. [29]. Combining these two contributions gives the red dashed line in Fig. 2(b), showing that Eq. (4) describes the data well. The pressure change along the melting curve dominates the capacitance change below 0.6 K; thermal expansion effects are more significant above 0.7 K, where $\alpha_v(T)$ is large. It is worth noting that the thermal expansion coefficient of ^{4}He on the melting curve is negative above 0.6 K [29–31], effectively causing contraction and increasing the liquid's density as the temperature rises.

The results of pure ^{4}He on melting curve demonstrate that our technique can precisely measure density variation due to both compression and thermal expansion. It enables us to evaluate these two effects and correct for them when applying this technique to monitor the concentration of isotopic impurities.

III. DISTRIBUTION OF ^{3}He IN LIQUID-SOLID COEXISTING SAMPLES

We then applied this technique to study the concentrations and motion of ^{3}He impurities when liquid and solid helium coexist. It is well known that when liquid and solid phases coexist, the equilibrium impurity concentrations in the two phases are different. This is the basis for the "zone refining" process used to produce very high purity metal or semiconducting crystals. For helium, a ^{3}He atom's energy is lower in liquid than in solid ^{4}He, so its equilibrium concentration is smaller in the solid. The relative binding energy in the liquid is 1.36 K, so the ratio of equilibrium concentrations in the liquid and solid, x_{3l}/x_{3s}, increases rapidly as temperature decreases, becoming larger than 10^{20} at 20 mK [32]. At such temperatures, equilibrium coexistence is essentially between a pure ^{4}He solid and a liquid in which all the ^{3}He impurities are dissolved. ^{3}He impurities' binding to liquid-solid interfaces is even stronger, and their local areal concentration could be extremely high. However, its influence on the bulk liquid and solid concentrations is negligible due to the small number of binding sites on the interfaces.

To apply the capacitive technique to measure variations of ^{3}He concentration, we prepared liquid-solid coexisting samples with higher concentrations x_3 of 1000, 2000, and 3000 ppm. For each concentration, samples were prepared with two different solid fractions. To prepare each sample, the experimental cell was first emptied by pumping at 20 K for 24 h to remove ^{3}He before cooling to 1 K. After a calibrated amount of ^{3}He gas was dosed into the cell, it was filled with pure liquid ^{4}He ($x_3 = 120$ ppb), kept at 2.4 K, and pressurized to between 30 and 35 bar. It was then rapidly cooled to 1 K in order to form a solid block in the capillary which prevented ^{3}He impurities from exiting the cell. The cell was further cooled by operating the dilution refrigerator to its base temperature (16 mK). The initial liquid pressure (between 30 and 35 bar) determined the final solid fraction (between 20% and 52% by volume). All samples were held at 16 mK for more than 4 h before being slowly warmed up.

The temperature was slowly ramped from 16 to 850 mK at a rate of $\frac{dT}{dt} = 2.5$ mK/min, and the entire process took about 6 h. It has been shown in previous NMR experiments that diffusion of ^{3}He impurities in solid ^{4}He can be slow, lasting for more than 10 h at 8 mK [33]. Therefore, the samples in our experiments were not necessarily at equilibrium during the temperature ramps. However, we did not conduct extremely slow temperature ramps to ensure equilibrium since our goal is to apply this technique in monitoring ^{3}He's concentration change and their migration, which are already obvious before equilibrium is reached.

Figure 3(a) shows the liquid pressure during temperature ramps for different samples. Melting pressures are significantly changed from that for pure ^{4}He and share some common features: (1) Melting pressures at the lowest temperature are shifted relative to that for pure ^{4}He; (2) they increase with temperature, reaching a broad maximum at around 300 mK, and then decrease up to 850 mK; (3) they drop below the value for pure ^{4}He at $T > \approx 600$ mK. These features are more prominent for larger x_3 and for higher solid fraction f.
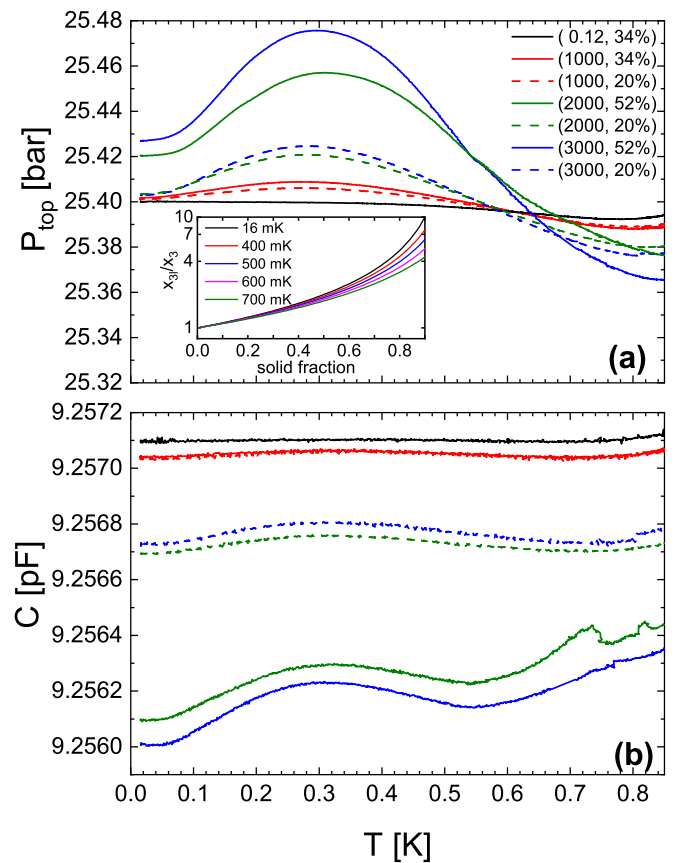

FIG. 3. (a) Liquid pressure measured during temperature ramps for solid-liquid coexisting samples. Numbers in the parentheses label the overall average ^{3}He concentration (in ppm) and the solid fraction for each sample. Inset: Calculated normalized ^{3}He concentrations in the liquid phase, x_{3l}/x_3, as a function of the solid fraction for various temperatures. (b) Simultaneous measurements of capacitance during the temperature ramps. The anomalous increases and sudden decreases for the sample (2000 ppm, 52%) above 0.6 K are likely due to temporary crystallization of solid within the capacitor gap.

^{3}He impurities are known to affect the melting curve of ^{4}He. At zero temperature, the ^{3}He atoms move to the liquid, where they form a dilute Fermi liquid in equilibrium with a pure ^{4}He solid. The ^{3}He produces an osmotic pressure in the liquid that raises the melting curve pressure, even at zero temperature [20]. At low temperatures, the entropy S_l of dilute ^{3}He is linear in T and is much larger than the T^3 phonon entropy S_s of the solid ^{4}He. This produces a melting curve with a pressure increase proportional to T^2. At higher temperatures, ^{3}He dissolves into the solid, giving it an increasing ^{3}He spin entropy in addition to its phonon entropy. At about 300 mK, the melting curve has a maximum where the solid and liquid entropies are equal, and then has a negative slope at higher temperatures where $S_s > S_l$. At about 0.6 K the melting pressure drops below that of pure ^{4}He, reaching a minimum around 1 K and then increasing again at higher temperatures.

The data in Fig. 3(a) show these features and are qualitatively consistent with earlier melting curve experiments with larger ^{3}He concentrations [18–20]. Those experiments involved samples with very small solid fractions, f. This meant that the "zone refining" in solid has negligible effect, and the ^{3}He concentration in liquid, x_{3l}, was essentially equal to the nominal (overall average) concentration, x_3, and independent of temperature. Because of the larger solid fractions in our experiments (between 20% and 52%), the concentration in the liquid phase x_{3l} increases significantly when ^{3}He leaves the solid at low temperatures. At zero temperature, all the ^{3}He would be in the liquid, with a concentration $x_{3l} = \frac{x_3}{(1-f)}$. In the sample with the largest solid fraction, $f = 0.52$, and an overall ^{3}He concentration of 3000 ppm, x_{3l} is about 6250 ppm at the lowest temperature. When the temperature is raised, ^{3}He migrates from the liquid to the solid and x_{3l} decreases, approaching x_3 at high temperature. This means that x_{3l} is not constant in our measurements so the temperature dependences of the pressure cannot be quantitatively compared to earlier work at constant x_{3l} [18–20].

The increase in the melting pressure at low temperature can be compared to the values in the work of Samela *et al.* [20]. Their lowest ^{3}He concentration was 6200 ppm, nearly the same as the low temperature concentration in the liquid for our highest ^{3}He concentration sample with 52% solid. However, the pressure shift in Fig. 3(a) for this sample (27 mbar) is much larger than the corresponding value in Ref. [20], about 7 mbar. The pressure shifts for samples with 20% solid are in much better agreement with the earlier work. It should be noted that, with $dP/dT > 0$, cooling to its lowest temperature freezes partial liquid to solid. Under a constant-density condition, crystallization can take place not necessarily from the solid surface but anywhere as long as nucleation condition is locally met. Thus, the liquid pressure gauge could be partially or fully covered by the solid even though the average solid fraction is controlled below (but close to) 60%. Previous studies have shown that solid helium can sustain certain amount of stress [34]. Thus, the discrepancy between our results and Ref. [20] could be ascribed to the stress gradients in the larger solid fraction sample that create pressure offsets at low temperature.

The results of simultaneous measurements of the capacitance in the liquid phase are shown in Fig. 3(b). Because of the larger effective atomic volume of ^{3}He impurities, the dielectric constant (capacitance) is reduced by an amount proportional to x_{3l}. The capacitance decreases are larger for samples with larger solid fractions, as expected given the higher ^{3}He concentrations when ^{3}He atoms migrate from the solid to the liquid. In addition to these ^{3}He concentration effects, the capacitance curves have broad maxima around 0.3 K, reflecting the compression of the liquid due to the pressure maxima in Fig. 3(a). Aside from this pressure effect, the capacitances increase monotonically with temperature, reflecting the decrease in x_{3l} as ^{3}He impurities migrate from the liquid back to the solid phase as the temperature rises.

The ^{3}He concentrations in the liquid and solid phases can be estimated as

$$x_{3l}(f, T) = x_3 \frac{1}{R(T)f + (1 - f)}, \qquad (5)$$

$$x_{3s}(f, T) = x_3 \frac{R(T)}{R(T)f + (1 - f)}, \qquad (6)$$

where $R(T) = x_{3s}/x_{3l}$. Although ^{3}He atoms in liquid ^{4}He are fermionic quasiparticles, our measurements were made above the Fermi temperatures of such dilute mixtures, and the ^{3}He can be treated using a Boltzmann distribution with $R(T) = e^{\Delta E/k_B T}$, where $\Delta E/k_B = -1.36$ K. The inset of Fig. 3(a) shows the normalized ^{3}He concentrations in the liquid, x_{3l}/x_3, calculated as a function of solid fraction for different temperatures. These show that x_{3l} increases with f and decreases as the temperature increases. We can correct the capacitance curves for the melting curve pressure effect and roughly estimate x_{3l} in liquid phase. For the sample with the largest changes (3000 ppm ^{3}He, 52% solid), the resulting ^{3}He concentration x_{3l} is ≈ 8000 ppm at 16 mK, and it decreases to ≈ 5000 ppm at 0.7 K. This is in rough agreement with the values predicted by Eqs. (5) and (6): 6240 and 5400 ppm at 16 mK and 0.7 K, respectively.

IV. MIGRATION OF ^{3}He IN LIQUID-SOLID COEXISTING SAMPLES

Our main goal in these experiments was to measure the dynamics of ^{3}He migration in samples with coexisting solid and liquid phases. Since the equilibrium distribution of ^{3}He impurities is temperature dependent, they move between the solid and the liquid when the temperature is varied, changing x_{3l}. We can monitor the migration process by measuring the evolution of the melting curve pressure and the capacitance in the liquid phase. However, during the slow temperature ramps described in the previous section, the capacitance changes due to impurity migration are mixed with contributions from pressure changes and thermal expansion. Although it is possible to subtract the pressure contribution using the simultaneous measurements of the melting curve pressure, there is no direct and independent measurement of thermal expansion, so it is hard to correct for it or to distinguish it from the temperature dependence of the ^{3}He concentration in the liquid. To avoid this difficulty, we rapidly warmed the samples from the 16 mK base temperature where essentially all the ^{3}He is in the liquid to a higher temperature setpoint, and then monitored the evolution of the pressure and capacitance once temperature stabilized. The thermal expansion and melting curve pressure changes directly related with temperature change occur
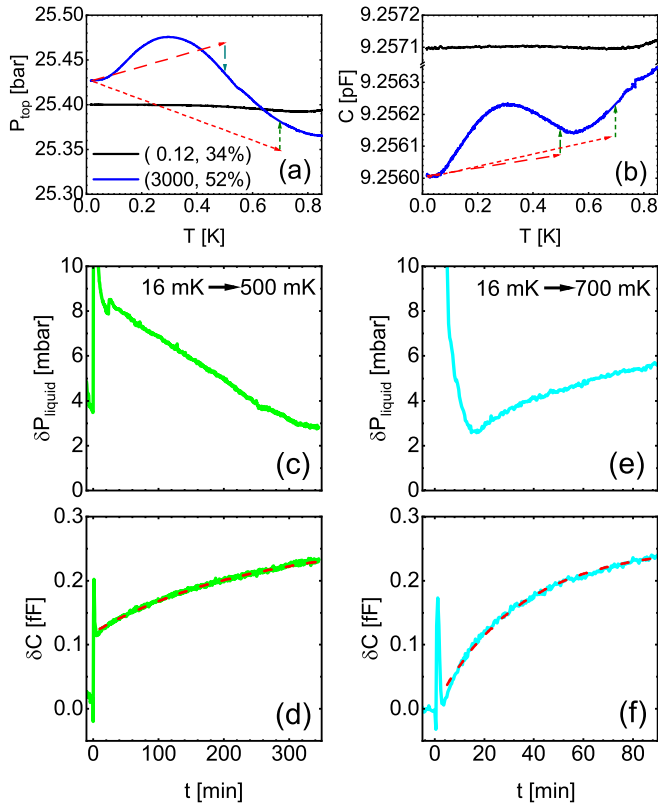
FIG. 4. Evolutions of pressure and capacitance after rapid warming. [(a), (b)] Trajectories of fast warmings followed by slow evolutions for the sample (3000 ppm, 52%). Pressure and capacitance data are the same as in Fig. 3, plotted here for reference. Red arrows represent the rapid warmings from 16 mK to higher temperature set points (500 and 700 mK); green arrows represent the slow evolutions after thermal equilibrium is reached. Evolutions of pressure and capacitance are plotted in panels (c) and (d) for $T = 500$ mK and in panels (e) and (f) for $T = 700$ mK. Reference values for the pressure changes in panels (c) and (e) are arbitrarily chosen; the capacitance changes are plotted with respect to the values immediately before the rapid warmings ($t = 0$). Red dashed lines in panels (d) and (f) are fittings by Eq. (7).

rapidly during heating. The ^{3}He migration is much slower so the concentration in the liquid, x_{3l}, is initially close to its low temperature value, i.e., larger than the equilibrium value at the higher temperature. The evolution of the pressure and capacitance after the temperature is raised reflects the time dependence of x_{3l} as some of the ^{3}He migrates from the liquid back to the solid to re-establish equilibrium.

We studied the ^{3}He migration for two samples (2000 ppm, 52%, and 3000 ppm, 52%), respectively. Figure 4 shows the results for the 3000-ppm sample. As indicated by the dashed red arrows in Figs. 4(a) and 4(b), at time $t = 0$ the temperature was quickly raised from 16 mK, reaching the higher temperature [either 500 mK in Figs. 4(c) and 4(d) or 700 mK in Figs. 4(e) and 4(f)] within 2 min. The endpoints of the red arrows in Figs. 4(a) and 4(b) schematically indicate the pressures and capacitances corresponding to the low-temperature ^{3}He concentrations, which are off from the equilibrium concentrations at 500 or 700 mK. There are sudden jumps of pressure and capacitance due to temperature changes. Once
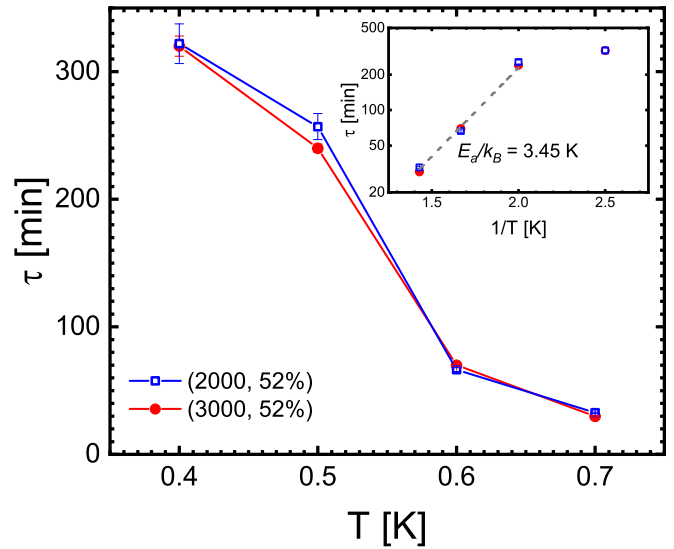

FIG. 5. Temperature dependence of migration time constant τ for samples (2000 ppm, 52%) and (3000 ppm, 52%). τ is extracted by fitting capacitance evolutions using Eq. (7). Inset: Arrhenius plot of τ vs $1/T$. The dashed line represents fitting $\tau = \tau_0 e^{E_a/k_B T}$, with an activation energy is extracted $E_a/k_B = 3.45$ K.

the temperature stabilizes, these jumps are followed by slow relaxations toward their equilibrium values at each temperature, as indicated by the green arrows in Figs. 4(a) and 4(b).

The capacitance following each jump increases with time for all temperatures, reflecting the decrease in x_{3l} as ^{3}He migrates from the liquid to the solid. The pressure decreases with time at 500 mK but increases at 700 mK, the expected evolution toward the equilibrium melting curve as x_{3l} decreases. Similar measurements were performed with temperature setpoints at 400 and 600 mK, with results consistent with the description above. In principle, it would also be possible to monitor ^{3}He migrating in the opposite direction, from the solid to liquid after a sudden reduction in temperature. However, this is not feasible in practice because of the relatively slow cooling rate of the dilution refrigerator.

Except for the initial jumps due to rapid heating, the pressure changes are less than 5 mbar for all temperatures. The capacitance changes corresponding to liquid compression or expansion by a 5-mbar pressure change are less than 10 aF, much smaller than the capacitance changes shown in Figs. 4(d) and 4(f). This implies that the observed capacitance evolutions at 500 and 700 mK are dominated by variations of x_{3l}. The relaxation of the ^{3}He concentrations can be described by

$$\delta C(t) = \delta C_0 (1 - e^{-(t-t_0)/\tau}), \qquad (7)$$

where C_0 is a fitting parameter, and t_0 is the time for samples to reach *thermal* equilibrium—shorter than 5 min for all fits. The characteristic time constant τ for ^{3}He migration can be extracted from the fits. The temperature dependence of τ is shown in Fig. 5 for the two samples. The time constants are essentially the same for the two different ^{3}He concentrations and decrease from $\approx$320 min at 400 mK to $\approx$30 min at 700 mK. This trend is qualitatively consistent with previous NMR studies which showed that it takes tens of hours for

^{3}He impurity concentrations to equilibrate within solid ^{4}He at 8 mK [33]. A longer time constant would be expected in these NMR experiments, given their much lower temperature. Temperature dependence of τ above 0.5 K can be fitted by a thermally activated process (see inset of Fig. 5). The activation energy $E_a/k_B = 3.45$ K is smaller but still comparable with previous NMR experiments [35,36] on ^{3}He diffusion in solid ^{4}He above 1 K. τ deviates from the trend of thermal activation at 0.4 K, also similar to NMR experiments which show a constant diffusion rate at lower temperatures, due to quantum tunneling.

Note that, given these long time constants, it is unlikely that the melting pressure and capacitance curves in Fig. 3 correspond to equilibrium ^{3}He concentrations, particularly at low temperatures and for the samples with the largest solid fraction.

The long time constants for ^{3}He migration are not associated with diffusion in the liquid. Neutron scattering experiments measured diffusion coefficients for ^{3}He in liquid ^{4}He (with $x_3 \approx 1000$ ppm). They had roughly a T^{-7} dependence, with values ranging from ≈ 1 cm^2/s at 1 K to ≈ 100 cm^2/s at 0.5 K [37]. Given the dimension of our experimental cell ($L \approx 1$ cm), the diffusion equilibrium time within the liquid phase, $t = \frac{L^2}{2D}$, is less than 1 s. This is several orders of magnitude faster than our observed relaxation rates, so the bottleneck for ^{3}He migration must either be in the solid phase or at the liquid-solid interface.

Diffusion of ^{3}He within solid ^{4}He is highly dependent on temperature and molar volume. It is also limited by scattering from ^{3}He impurities and other defects. For solid ^{4}He close to its melting pressure, D can vary by over four orders of magnitude below 0.5 K, from 10^{-7} cm^2/s for $x_3 = 60$ ppm to 10^{-11} cm^2/s for $x_3 = 5\%$ [36]. Ballistic motion of ^{3}He atoms via quantum tunneling is the main diffusion mechanism for low temperatures and dilute concentrations [38]. At higher concentrations, ^{3}He-^{3}He scattering via their elastic interactions becomes important and reduces diffusion [35,36]. For $T > 1.5$ K, ^{3}He-phonon interactions dominate and the diffusion constants for different ^{3}He concentrations converge. In this range, D decreases with increasing temperature [36].

For the sample of Fig. 4 (3000 ppm, 52%), the ^{3}He concentration in the solid phase can be estimated as $x_{3s} < 200$ ppm in the temperature range between 400 and 700 mK. This is in the dilute scattering region (the same for the sample with 2000 ppm, 52%) where D would be on the order of 10^{-7} cm^2/s [36]. The corresponding diffusion time $t = \frac{L^2}{2D}$ in the solid would then be about 5×10^6 s, two orders of magnitude longer than our observed relaxation times in the liquid. However, ^{3}He diffusion in solid can be facilitated by defects. ^{3}He atoms tend to bind to dislocation cores as the lattice mismatch provides larger volume to accommodate ^{3}He atoms [2,3,39,40]. It has been pointed out that ^{3}He atoms can transport along cores more rapidly than in pristine lattices [41]. Such a "pipe diffusion" effect is not unique to solid helium but has also been observed in classical solids [42]. However, given a typical dislocation density of 10^6 cm^{-2}, dislocations in 1-cm^3 solid ^{4}He can only accommodate 5×10^{-11} mol ^{3}He atoms, accounting for only 1 ppb of ^{3}He concentration, more than 10^5 times lower than the actual ^{3}He concentration in solid. Therefore, an extremely high diffusion speed (about 0.5–5 m/s) is required for pipe diffusion to be the dominant mechanism, which is not likely in our experiments. In comparison, grain boundaries can accommodate many more impurities and are well known to facilitate impurity motion as "sheet diffusion" [43]. It has been proposed that grain boundaries as well as interfaces between solid helium and walls are in two-dimensional liquid nature [44,45]. They provide interconnecting channels for ^{3}He to penetrate into solid, effectively multiplying solid-liquid interfaces. Taking 50 μm as a typical grain size (in cubic shape), the area of grain boundaries in a 1-cm^3 solid ^{4}He is 600 cm^2. It can accommodate 1 mmol ^{3}He, equivalently 20 ppm. This fraction is non-negligible in comparison with the total ^{3}He concentration in solid, making "sheet diffusion" along grain boundaries a possible mechanism for the diffusion of ^{3}He in solid. Our results hint at a thermal activation energy smaller than that seen in NMR experiments above 1 K, suggesting that the diffusion of ^{3}He is not just via exchange with vacancies in the bulk solid.

The liquid-solid interface could also be a bottleneck for ^{3}He diffusion. The interface strongly attracts ^{3}He atoms (with a binding energy of 2–10 K relative to liquid [46]). The local ^{3}He concentration on an interface is about 25% for the first adsorbed layer at ≈ 1 K [46], and could be close to unity at lower temperatures. Given its fermionic statistics, such a ^{3}He layer creates a barrier, potentially slowing down the migration of ^{3}He from liquid to solid. Also, ^{3}He atoms behave as narrow-band quasiparticles in solid phase and there could be a significant reflection probability at the interface, reducing their chance of entering the solid. However, it is not possible to extract a time constant for ^{3}He atoms to cross the interface from our data, given the uncertainties about diffusion times within the solid.

V. SUMMARY

To summarize, we developed a convenient technique to monitor ^{3}He concentration in liquid ^{4}He. By developing a concentric cylindrical capacitor and using a commercial capacitance bridge, we are able to resolve 40 ppm change in ^{3}He concentration. Using this technique, we successfully observed ^{3}He impurities concentrating in the liquid phase at low temperatures in liquid-solid coexisting samples and monitored their migration from liquid to solid phase when the temperature was raised. The migration process became faster as the temperature increased, with a characteristic time constant ranging from ≈ 320 min at 0.4 K to ≈ 30 min at 0.7 K. The slow migration process is due to diffusion of ^{3}He impurities within the solid ^{4}He and there may be an additional bottleneck for transmission through liquid-solid interfaces.

[1] D. S. Greywall, Specific Heat of Dilute Solutions of ^{3}He in ^{4}He and the ^{3}He-Quasiparticle Excitation Spectrum, Phys. Rev. Lett. **41**, 177 (1978).

[2] J. Day and J. R. Beamish, Low-temperature shear modulus changes in solid ^{4}He and connection to supersolidity, Nature (London) **450**, 853 (2007).

[3] A. Haziot, X. Rojas, A. D. Fefferman, J. R. Beamish, and S. Balibar, Giant Plasticity of a Quantum Crystal, Phys. Rev. Lett. **110**, 035301 (2013).

[4] F. Souris, A. D. Fefferman, A. Haziot, N. Garroum, J. R. Beamish, and S. Balibar, Search for dislocation free helium 4 crystals, J. Low Temp. Phys. **178**, 149 (2015).

[5] Z. G. Cheng and J. Beamish, Defect motion in a quantum solid with spin: hcp ^{3}He, Phys. Rev. B **95**, 180103(R) (2017).

[6] Y. Vekhov, W. J. Mullin, and R. B. Hallock, Universal Temperature Dependence, Flux Extinction, and the Role of ^{3}He Impurities in Superfluid Mass Transport through Solid ^{4}He, Phys. Rev. Lett. **113**, 035302 (2014).

[7] Z. G. Cheng, J. Beamish, A. D. Fefferman, F. Souris, S. Balibar, and V. Dauvois, Helium Mass Flow through a Solid-Superfluid-Solid Junction, Phys. Rev. Lett. **114**, 165301 (2015).

[8] Z. G. Cheng and J. Beamish, Compression-Driven Mass Flow in Bulk Solid ^{4}He, Phys. Rev. Lett. **117**, 025301 (2016).

[9] J. Shin and M. H. W. Chan, Extinction and recovery of mass flow through solid ^{4}He samples, Phys. Rev. B **101**, 014507 (2020).

[10] J. Shin, D. Y. Kim, A. Haziot, and M. H. W. Chan, Superfluidlike Mass Flow through 8 μm Thick Solid ^{4}He Samples, Phys. Rev. Lett. **118**, 235301 (2017).

[11] F. Souris, A. D. Fefferman, H. J. Maris, V. Dauvois, P. Jean-Baptiste, J. R. Beamish, and S. Balibar, Movement of dislocations dressed with ^{3}He impurities in ^{4}He crystals, Phys. Rev. B **90**, 180103(R) (2014).

[12] D. O. Edwards and S. Balibar, Calculation of the phase diagram of ^{3}He - ^{4}He solid and liquid mixtures, Phys. Rev. B **39**, 4083 (1989).

[13] X. Rojas, C. Pantalei, H. J. Maris, and S. Balibar, Acoustic properties of solid ^{4}He in the limit of zero impurity, J. Low Temp. Phys. **158**, 478 (2010).

[14] E. Rolley, S. Balibar, C. Guthmann, and P. Nozières, Adsorption of ^{3}He on ^{4}He crystal surfaces, Phys. B: Condens. Matter **210**, 397 (1995).

[15] J. Treiner, Helium mixtures on weak binding substrates, J. Low Temp. Phys. **92**, 1 (1993).

[16] A. Y. Parshin, Low temperature mobility of steps on the ^{4}He crystal facets: Effects of ^{3}He impurities, J. Low Temp. Phys. **110**, 133 (1998).

[17] C.-L. Wang and G. Agnolet, Effects of ^{3}He impurities on the ^{4}He solid-liquid interface, J. Low Temp. Phys. **89**, 759 (1992).

[18] V. N. Lopatik, Crystallization curves for weak ^{3}He - ^{4}He solutions at low temperatures, Sov. Phys. JETP **59**, 284 (1984).

[19] Yu. D. Anufriev, V. N. Lopatik, and A. P. Sebedash, Crystallization curves for weak ^{3}He - ^{4}He solutions at low temperatures, JETP Lett. **37**, 45 (1983).

[20] A. Salmela, A. Sebedash, J. Rysti, E. Pentti, and J. Tuoriniemi, Osmotic pressure of ^{3}He/^{4}He mixtures at the crystallization pressure and at millikelvin temperatures, Phys. Rev. B **83**, 134510 (2011).

[21] A. P. Sebedash, J. T. Tuoriniemi, E. M. M. Pentti, and A. J. Salmela, Osmotic pressure of ^{3}He - ^{4}He solutions at 25.3 bar and low temperatures, J. Low Temp. Phys. **150**, 181 (2008).

[22] E. Pentti, J. Tuoriniemi, A. Salmela, and A. Sebedash, Melting pressure thermometry of the saturated helium mixture at millikelvin temperatures, J. Low Temp. Phys. **146**, 71 (2006).

[23] J. Rysti, M. S. Manninen, and J. Tuoriniemi, Measurements on melting pressure, metastable solid phases, and molar volume of univariant saturated helium mixture, J. Low Temp. Phys. **175**, 739 (2014).

[24] M. S. Manninen, Oscillations on helium surfaces, Ph.D. thesis, Aalto University, Espoo, Finland, 2015.

[25] E. C. Kerr and R. H. Sherman, The molar polarizability of ^{3}He at low temperature and its density dependence, J. Low Temp. Phys. **3**, 451 (1970).

[26] H. A. Kierstead, Dielectric constant and molar volume of saturated liquid ^{3}He and ^{4}He, J. Low Temp. Phys. **23**, 791 (1976).

[27] M. Chan, M. Ryschkewitsch, and H. Meyer, The dielectric constant in liquid and solid ^{4}He, J. Low Temp. Phys. **26**, 211 (1977).

[28] C. Boghosian, H. Meyer, and J. E. Rives, Density, coefficient of thermal expansion, and entropy of compression of liquid helium-3 under pressure below 1.2 K, Phys. Rev. **146**, 110 (1966).

[29] I. A. Todoshchenko, H. Alles, H. J. Junes, M. S. Manninen, A. Y. Parshin, and V. Tsepelin, Elementary excitations in solid and liquid ^{4}He at the melting pressure, J. Low Temp. Phys. **150**, 258 (2008).

[30] E. R. Grilly, Pressure-volume-temperature relations in liquid and solid ^{4}He, J. Low Temp. Phys. **11**, 33 (1973).

[31] C. Boghosian and H. Meyer, Density, coefficient of thermal expansion, and entropy of compression of liquid ^{4}He under pressure below 1.4 K, Phys. Rev. **152**, 200 (1966).

[32] C. Pantalei, X. Rojas, D. O. Edwards, H. J. Maris, and S. Balibar, How to prepare an ideal helium 4 crystal, J. Low Temp. Phys. **159**, 452 (2010).

[33] R. Toda, P. Gumann, K. Kosaka, M. Kanemoto, W. Onoe, and Y. Sasaki, Simultaneous measurement of torsional oscillations and NMR of very dilute ^{3}He in solid ^{4}He, Phys. Rev. B **81**, 214515 (2010).

[34] A. Suhel and J. R. Beamish, Pressure gradients in solid ^{4}He: Thermal quenching and annealing, Phys. Rev. B **84**, 094512 (2011).

[35] R. A. Guyer, R. C. Richardson, and L. I. Zane, Excitations in quantum crystals (a survey of NMR experiments in solid helium), Rev. Mod. Phys. **43**, 532 (1971).

[36] V. N. Grigor'ev, Diffusion in solid helium, Low Temp. Phys. **23**, 3 (1997).

[37] S. K. Lamoreaux, G. Archibald, P. D. Barnes, W. T. Buttler, D. J. Clark, M. D. Cooper, M. Espy, G. L. Greene, R. Golub, M. E. Hayden, C. Lei, L. J. Marek, J.-C. Peng, and S. Penttila, Measurement of the ^{3}He mass diffusion coefficient in superfluid ^{4}He over the 0.45–0.95 K temperature range, Europhys. Lett. **58**, 718 (2002).

[38] A. Andreev and I. Lifshitz, Quantum theory of defects in crystals, Sov. Phys. JETP **29**, 1107 (1969).

[39] M. A. Paalanen, D. J. Bishop, and H. W. Dail, Dislocation Motion in hcp ^{4}He, Phys. Rev. Lett. **46**, 664 (1981).

[40] I. Iwasa and H. Suzuki, Sound velocity and attenuation in hcp ^{4}He crystals containing ^{3}He impurities, J. Phys. Soc. Japan **49**, 1722 (1980).

[41] X. Rojas, A. Haziot, and S. Balibar, Migration of ^{3}He impurities along dislocation lines in ^{4}He single crystals, J. Phys.: Conf. Ser. **400**, 012062 (2012).

[42] M. Legros, G. Dehm, E. Arzt, and T. J. Balk, Observation of giant diffusivity along dislocation cores, Science **319**, 1646 (2008).

[43] S. V. Divinski, O. A. Lukianova, G. Wilde, A. Dash, N. Esakkiraja, and A. Paul, High-entropy alloys: Diffusion, in *Reference Module in Materials Science and Materials Engineering* (Elsevier, Amsterdam, 2020).

[44] S. Sasaki, R. Ishiguro, F. Caupin, H. J. Maris, and S. Balibar, Superfluidity of grain boundaries and supersolid behavior, Science **313**, 1098 (2006).

[45] S. A. Khairallah and D. M. Ceperley, Superfluidity of Dense ^{4}He in Vycor, Phys. Rev. Lett. **95**, 185301 (2005).

[46] Y. Carmi, E. Polturak, and S. G. Lipson, Roughening Transition in Dilute ^{3}He / ^{4}He Mixture Crystals, Phys. Rev. Lett. **62**, 1364 (1989).